A new Azo-DMOF-1 MOF as a photo-responsive low-energy CO_2 adsorbent and its exceptional CO_2/N_2 separation performance in mixed matrix membranes

Journal:	*ACS Applied Materials & Interfaces*
Manuscript ID	am-2018-122617.R1
Manuscript Type:	Article
Date Submitted by the Author:	09-Sep-2018
Complete List of Authors:	Prasetya, Nicholaus; Imperial College London, Department of Chemical Engineering Ladewig, Bradley; Imperial College London, Department of Chemical Engineering

A New Azo-DMOF-1 MOF as a Photo-responsive Low-energy CO_2 Adsorbent and its Exceptional CO_2/N_2 Separation Performance in Mixed Matrix Membranes

Nicholaus Prasetya and Bradley P. Ladewig

Barrer Centre, Department of Chemical Engineering, Imperial College London, Exhibition Road, London SW7 2AZ, United Kingdom.

KEYWORDS. Metal-organic framework, gas separation, photo-responsive, carbon capture, Matrimid, PIM-1

ABSTRACT. A new generation-2 light-responsive metal-organic framework (MOF) has been successfully synthesized using Zn as the metal source and both 2-phenyldiazenyl terephthalic acid and 1,4-diazabicyclo[2.2.2]octane (DABCO) as the ligands. It was found that Zn-azo-dabco MOF (Azo-DMOF-1) exhibited a photo-responsive CO_2 adsorption both in static and dynamic condition because of the presence of azobenzene functionalities from the ligand. Further application of this MOF was evaluated by incorporating it as a filler in a mixed matrix membrane for CO_2/N_2 gas separation. Matrimid and polymer of intrinsic microporosity-1 (PIM-1) were used as the polymer matrix. It was found that Azo-DMOF-1 could enhance both the CO_2

permeability and selectivity of the pristine polymer. In particular, the Azo-DMOF-1 – PIM-1 composite membranes have shown a promising performance that surpassed the 2008 Robeson Upper Bound.

INTRODUCTION.

During the last decade, there is a growing interest in the development of metal-organic framework (MOF). As one of the emerging porous materials, MOF has numerous positive aspects such as high surface area, pore size tailorability and also chemical and thermal stability. Recently, there is also a growing interest in developing a responsive MOF that has different behavior depending on the stimulus that it receives from the surroundings. Various stimulants have been investigated such as pH,[1] temperature,[2] magnetic field[3] and light.[4] Among the stimulants, light-responsive MOFs have attracted considerable interest among the researchers. This might be attributed to the abundance and convenience of using light as the stimulant. Moreover, recent investigations have also shown that designing a light-responsive MOF is one of the promising approaches towards low-energy carbon capture and storage.[5-7]

Generally, light-responsive MOFs can be classified into three generations. The generation-1 relies on the host-guest interaction between the framework and photo-responsive guest molecule to achieve light-responsive ability. The drawback of this approach is the significant reduction of the MOFs pore size since most of them are occupied by the guest molecules. Meanwhile in generation-2 light-responsive MOFs, a light-responsive ligand is used to build the MOF. While generation-2 light-responsive MOFs have a light-responsive moiety that protrudes into the MOF's pores,[8-10] the generation-3 light-responsive MOFs utilizes a light-responsive ligand that becomes the main building block of the MOFs.[4, 6, 11] Both generation-2 and generation-3 are

considered to be more efficient in harvesting in light energy without overly reducing the surface area, and various light-responsive MOFs have been developed since then for applications ranging from drug delivery to CO_2 adsorption.

In this paper, we report a new generation-2 light-responsive MOF that uses Zn as the metal source and 2-phenyldiazenyl terephthalic acid and 1,4-diazabicyclo(2.2.2)octane as the ligands which we subsequently call Azo-DMOF-1 (DMOF-1 stands for dabco-MOF-1 for its parent structure). This work is inspired by one of the most widely investigated MOFs, namely $Zn(bdc)(dabco)_{0.5}$ (Dabco MOF or DMOF-1), which was firstly reported by Dybstev and co-workers in 2004.[12] Various studies have been conducted since then based on this framework focusing on various subjects such as adsorption application,[13] post-synthetic modification[14-17] and exploration on its flexible framework.[18-20] Among these studies, there was also a previous attempt to make this MOF photo-responsive by loading the framework with azobenzene compounds as the guest molecule.[21] The authors have successfully proven the ability of the azo-loaded DMOF-1 to be photo-responsive through nitrogen sorption isotherm and UV-induced change of PXRD pattern. After UV light irradiation, the azobenzene compounds inside the pore isomerizes to *cis*-form and some spaces in the pore are opened resulting in higher nitrogen uptake. However, as stated above, the main drawback of this approach is the significant reduction of the MOF surface area and the MOF might no be longer suitable for further application. Another approach has then been attempted using a fluoro-based photo-responsive ligand to build a generation-2 copper-based dabco MOF which is called $Cu_2(F_2AzoBDC)_2(dabco)$.[22] The MOF was then successfully produced as a thin film and used as a membrane. The *cis-trans* azobenzene switching phenomenon could be induced by irradiating the membrane with visible light at different wavelengths. The efficacy of the isomerization was

then evaluated by various experiments such as 1,4-butenediol uptake and photo-switching separation of ethene and propene from hydrogen.

Compared to the previous attempts, our approach is to directly use a photo-responsive ligand protruding into the pore and thus a photo-responsive MOF with relatively higher surface area could be obtained with satisfactory CO_2 uptake. We focus on applying this MOF firstly as a low-energy CO_2 adsorbent and then as a filler in a mixed matrix membrane for CO_2/N_2 separation since this approach is one of the best alternatives to apply porous materials for gas separation.[23-24] This is based on previous investigations showing the beneficial aspect of having azobenzene functionalities in a porous materials in improving CO_2/N_2 separation performance.[25-27]

RESULTS AND DISCUSSIONS.

Synthesis and characterization of Azo-DMOF-1

The Azo-DMOF-1 was synthesized following the synthesis condition of DMOF-1 MOF apart from changing the terephthalic acid to 2-phenyldiazenyl terephthalic acid that has a dangling azobenzene group. The hypothetical figure of the MOF building unit is presented in **Figure 1**(A). We hypothesize that the azobenzene moieties protruding into the MOF's pore were randomly oriented (our unsuccessful attempt to obtain the single crystal X-Ray diffraction (SCXRD) data for a single crystal concurs with this). This phenomenon was previously observed in PCN-123 where the authors suggest that random orientation of the azobenzene moiety also prevents them obtaining the SCXRD.[8] Azo-DMOF-1 crystallizes as a rod-shape crystal and the size could extend up to 5 μm as can be seen from the micrograph in **Figure 1(**B).

Powder X-Ray diffraction (PXRD) was then performed to characterize the crystallinity of the new MOF and the result is given in **Figure 1**(C). First of all, it could be seen that the PXRD pattern of the Azo-DMOF-1 is different compared with the calculated pattern of the DMOF-1 MOF. This might be caused by the presence of azobenzene group protruding into the pore of the MOF. It has been previously observed that the DMOF-1 framework is flexible upon the presence of the guest molecule.[12] Considering that our ligand contains azobenzene group, this could then lead to different crystal structure obtained for the Azo-DMOF-1. As a further evaluation, the PXRD diffractogram of the Azo-DMOF-1 was also compared with the benzene-loaded DMOF-1.[12] As can be seen in **Figure 1**(C), both diffractograms are now more comparable to each other. This finding could be explained by the presence of the benzene group protruding into the Azo-DMOF-1 framework that comes from the ligand. This benzene ring from the azo ligand could contribute in the similar way as the benzene compound loaded in the DMOF-1 framework resulting in a similar structure between the two MOFs. However, there is also a slight discrepancy as can be observed in the diffractograms at 2θ around 13° for the benzene-loaded DMOF-1 which corresponds to (2 0 0) plane. This peak was observed to be slightly shifted to lower angle for the Azo-DMOF-1 which might be caused by the random orientation of the azobenzene ligand inside the pore between the two MOFs.

Nitrogen sorption isotherm data was then collected to measure the surface area of the Azo-DMOF-1 and the result is presented in **Figure 1**(D). The Azo-DMOF-1 exhibits type-1 isotherm without any hysteresis indicating a microporous structure. The calculated BET surface area was found to be 581 $m^2 g^{-1}$. This value is significantly lower compared with the DMOF-1 synthesized using the same condition which was around 1500 $m^2 g^{-1}$ as can also be seen in **Figure 1**(D). This could be explained by the presence of the azobenzene group inside the pore that reduces the

surface area of the MOF as previously observed with DMOFs modified with various functionalities pendant to the ligand, protruding into the pore.[16, 28] The presence of azobenzene group also affected the pore volume and pore width of the Azo-DMOF-1. As could be seen in the inset of **Figure 1**(D), the pore width of Azo-DMOF-1 was slightly lower compared with the DMOF-1. The pore width of the former was found to be around 0.6 nm while the latter has a pore width around 0.7 nm. The more significant effect could be observed from the maximum pore volume. The pore volume of Azo-DMOF-1 was found to be around 0.3 $cm^3\ g^{-1}$ which is less than half of the value of the DMOF-1 which is around 0.79 $cm^3\ g^{-1}$. This indicates that the pores of Azo-DMOF-1 were largely occupied with the azobenzene moiety resulting in a significant pore volume reduction.

CO_2 adsorption experiment was then conducted to measure the uptake capacity of the Azo-DMOF-1 and also to investigate its dynamic photoswitching which is applicable for low energy CO_2 capture. First of all, it could be seen from **Figure 2**(A) and (B) that at 750 mmHg, the CO_2 uptake capacity of Azo-DMOF-1 was found to be around 73 and 41 $cm^3\ g^{-1}$ STP at 273 and 298 K, respectively. Interestingly, this uptake capacity is not significantly different compared with the CO_2 uptake of DMOF-1 which we found around 43 $cm^3\ g^{-1}$ STP at 298 K. This behavior was also previously observed in the functionalized DMOF-1 family with chlorine and hydroxyl functionalities that did not experience CO_2 uptake reduction at 1 bar compared with the DMOF-1.[29] In spite of the fact that Azo-DMOF-1 has lower surface area than DMOF-1, it does seem that at low relative pressure (P/P0), the CO_2 uptake is not affected by the surface area of the MOFs. It has been previously studied that in an empty DMOF-1, regardless of the functionalities in the terephthalate, the lowest energetic site of the DMOF-1 is the area close to the metal site where CO_2 is most favorably adsorbed.[29] This site could also be the most favorable site for CO_2

adsorption for Azo-DMOF-1 at low relative pressure. And from this study, it could be then indicated that the functionalization of the terephthalate with azobenzene does not seem to disturb this region resulting in comparable total CO_2 uptake between Azo-DMOF-1 and DMOF-1 at 750 mmHg and 298 K. Previous computational study in light-responsive PCN-123 using the same photo-responsive ligand also indicate that regardless of the azobenzene orientation in the pore, it does not significantly shield the area around metal center where CO_2 is most favorably adsorbed.[30] Thus, the assumed random orientation of the azobenzene in Azo-DMOF-1 does not also affect the total CO_2 adsorption at this condition. However, as the pore of the Azo-DMOF-1 are more occupied with CO_2, the impact of the bulky azobenzene ligand could be observed. As can be seen in the CO_2 uptake data at 273 K, the CO_2 uptake of Azo-DMOF-1 was lower than the DMOF-1 at 750 mmHg. The total uptake at 750 mmHg and 273 K was found to be around 73 and 90 cm^3 g^{-1} (STP) for Azo-DMOF-1 and DMOF-1, respectively. This then indicates that at higher relative pressure (P/P0), as more CO_2 molecules could be adsorbed, lower pore volume and surface area of Azo-DMOF-1 than DMOF-1 starts to significantly limit the total amount of CO_2 that can be adsorbed.

Since the MOFs pores are occupied with azobenzene functionalities, a CO_2 photo-responsive ability of the MOF was also investigated. As can be seen in **Figure 2**(A) and (B), the CO_2 uptake of the Azo-DMOF-1 MOF was lower when it was measured under UV-light under static condition. The CO_2 uptake under UV light at 750 mmHg was found to be around 36 and 29 cm^3 g^{-1} STP at 273 and 298 K, respectively. This value was around 30% lower compared with the normal condition. In addition, Azo-DMOF-1 could also experience a CO_2 dynamic photoswitching as previously observed with generation-3 light-responsive MOFs.[6, 11] This behavior was not previously observed in PCN-123 as a generation-2 light-responsive MOF.[8]

Upon UV light irradiation, the CO_2 adsorption of the MOF decreased significantly to be about 35% from its non-UV irradiated condition that intersects well with the CO_2 uptake under UV-light in static condition. Once the UV light was switched off, the CO_2 uptake could be brought back to its initial condition. We also did a control experiment using the DMOF-1 since the only difference is the presence of azobenzene group inside the pore. As can be seen in the supporting information (Figure S6), although we did observe a slight decrease in CO_2 uptake when the UV light was switched on, this could be attributed to the slight increase in temperature generated from the UV light. However, this decrease was not as significant as observed in the Azo-DMOF-1.

The difference in CO_2 uptake under UV irradiation could then be attributed to the hindered isomerization of the azobenzene group inside the MOF's pores as previously observed in F-azo-MIL-53.[31] In this phenomenon, the energy from UV light could be absorbed by the azobenzene groups of the MOF. However the pore condition might hinder them to isomerize efficiently. This was also proven through UV-Vis spectrum of the digested sample (Supporting Information, Figure S7). As could be seen, almost no absorbance change was observed when the solid state MOF was irradiated with UV light followed by digestion. However, a typical azobenzene isomerization could be observed if the sample was digested first followed by UV irradiation. Since the UV light energy received by the MOF could not be utilized to isomerize the azobenzene ligand, the energy must be dissipated through release of adsorbed CO_2 from the framework. This explanation is more likely since no significant difference in CO_2 uptake was observed when the MOF was irradiated *ex-situ* which was then followed by CO_2 uptake measurement (Supporting Information, Figure S8). This showed that no photoisomerzation of the azobenzene group occurred after the UV-light irradiation.

An evaluation on the CO_2 isosteric heat of adsorption (Q_{ads}) also confirms the low CO_2-MOF framework interaction when it was irradiated with UV light. From **Figure 2**(C), it could be seen that under normal condition, the Q_{ads} of CO_2 was found to be around 25 kJ mol^{-1}. This value is higher compared with the Q_{ads} reported for DMOF-1 MOF which is around 17-18 kJ/mol as what we also observed (Supporting Information, Figure S10) [32-33] but comparable with other DMOF-1 framework that has favorable CO_2 adsorption site[29] and other potential porous materials for carbon capture such as Cu-BTC[32, 34] This proves that the presence of azobenzene group from the ligand also contributes in improving the interaction between CO_2 and the MOF framework. This might be caused by the ability of the azobenzene functionality to establish a Lewis acid-base interaction with CO_2 molecule and thus improving the Azo-DMOF-1 framework affinity towards CO_2.[35] From carbon capture point of view, this value can be considered as moderate which is beneficial in the trade-off between selectivity and energy required for regeneration.[33-34] Meanwhile, under UV-irradiation, the Q_{ads} was found to be around 18 kJ mol^{-1} which is around 30% lower compared with the non-irradiated state and comparable with non-functionalized DMOF-1. Lower Q_{ads} value could then be related with lower affinity between CO_2 and the framework induced by the UV light resulting in instantaneous CO_2 release upon UV irradiation. Combination of lower CO_2 uptake and CO_2 Q_{ads} during UV irradiation then make this material to be promising for a low-energy carbon capture application with minimal regeneration energy requirement.

As a last evaluation, the MOF was then tested for its stability during storage and adsorption cycling. During this study period, the MOF was stored in a laboratory ambient condition (without using any glove box or inert condition) for one month and had two further dynamic CO_2 photo-switching tests. The result is presented in **Figure 2**(D). The aged MOF could still maintain

its CO_2 uptake after storing as in the fresh condition. Furthermore, it could also maintain its highly efficient dynamic photoswitching ability as observed in its pristine condition. This shows the framework structure of the MOF could still be well maintained during the storing condition and no indication of structural degradation was observed as also confirmed by PXRD pattern of the aged MOF when stored for two weeks and four weeks (Supplementary Information, Figure S9). The combination of relatively high CO_2 uptake, highly efficient CO_2 dynamic photoswitching and relative stability of the Azo-DMOF-1 renders it to be one of the best performing generation-2 light-responsive MOFs studied this far (see Table S1 for a performance comparison) and makes it a promising candidate for low energy CO_2 capture.

Azo-DMOF-1 mixed matrix membrane

To further explore the application of the MOF, we further utilized the MOF to be incorporated as filler in a mixed matrix membrane and to evaluate the performance of the resulting mixed matrix membrane for CO_2/N_2 separation. This is mainly because previous works have shown the beneficial aspect of having azobenzene functionality in enhancing the CO_2/N_2 separation in membrane-based separation.[36-37] Matrimid and PIM-1 were then chosen as the polymer matrix for the MMM and the MOF was loaded with various loadings between 5 to 20 wt%. We found that we could not obtain a very high loading of the MMM since the structure of the resulting MMM started to be very brittle at a very high loading. This might be caused by the particle size of the MOFs that is still in the range of the micron-size.

All the MMMs were then characterized using various methods such as PXRD, FTIR, TGA and SEM to confirm to presence of the MOF inside the matrix. The results are presented in **Figure 3**. It could be seen from the PXRD results that the peaks belonging to the Azo-DMOF-1 start to

appear at 5 wt% loading both for Matrimid and PIM-1 composite membrane. The relative intensity of these identity peaks increase as the MOF loading is increased in both composite membranes accompanied by decrease in relative intensity of the peaks belonging to the polymer matrix. It is also observed that the main peaks from the Azo-DMOF-1 were slightly shifted to lower angle. This could be attributed to the polymer chain penetration into the Azo-DMOF-1 pore as previously observed in the glassy polymer with MOF with flexible structure.[38]

FTIR spectra also confirm the presence of the MOF inside the composite membranes as the azobenzene peaks could be observed in the MMMs spectra. Three peaks belong to the azobenzene could be observed in the MMMs, namely at around 1374 cm^{-1}, 1398 cm^{-1} which are attributed to N=N stretch and 1636 cm^{-1}. These peaks could be attributed to the azobenzene compound inside the matrix.

Thermal analysis of MMMs also showed the incorporation of the MOFs inside the polymer matrix. As in DMOF-1, azo-DMOF-1 also started to experience degradation at around 300^{o}C until around 450^{o}C. This was indicated by two regions which can be attributed to the degradation of the two linkers used in the MOF. As in the MOF, all MMMs also exhibited a similar behavior and much more pronounced at higher loading, namely the 20 wt% azo-DMOF-1 – PIM-1 polymer.

Lastly, it could also be seen from the SEM micrographs that the MOF particle could be evenly dispersed inside the MMMs. No interfacial defects between the MOFs and polymer were observed from the micrographs indicating a good interaction could be established between the MOF and the polymer at the loadings used in this study. However, some particle aggregates

could be appreciated to appear for the PIM-1 MMM with the highest loading which could impact the membrane performance.

The performance of the MMMs was then evaluated for CO_2/N_2 separation which is applicable in post-combustion carbon capture. The first composite membrane to be evaluated was Azo-DMOF-1 – Matrimid MMM. As can be seen in **Figure 4**(A), both CO_2 permeability and CO_2/N_2 selectivity could be significantly enhanced. The CO_2 permeability of the pristine Matrimid was found to be about 6.7 Barrer whilst CO_2/N_2 ideal selectivity was around 29. Upon loading the Matrimid with 5 wt% of Azo-DMOF-1, the CO_2 permeability could be increased to around 9.6 Barrer while the increase in CO_2/N_2 ideal selectivity reached 36. For Matrimid MMM with the highest loading of 10 wt%, the improvements were more pronounced. The CO_2 permeability increased about twofold to be about 13 Barrer accompanied by an increase in CO_2/N_2 ideal selectivity to around 50. To confirm that this effect was due to the presence of the Azo-DMOF-1, we also did an evaluation by fabricating a 10 wt% DMOF-1 – Matrimid MMM. As can be seen in **Figure 4**(A), the Matrimid MMM loaded with DMOF-1 MOF did also exhibit improvement in CO_2 permeability but its CO_2/N_2 ideal selectivity barely increased.

Apart from Matrimid as the most common polymer, we also studied the performance of this MOF using PIM-1 as the polymer matrix to fabricate MMMs. This is because pristine PIM-1 membrane has a promising combination of gas permeability and selectivity which is close to the 2008 Robeson Upper Bound for most gas pairs. As in Matrimid-based MMM, we also varied the loading of the Azo-DMOF-1 in PIM-1 from 5 to 20 wt% loading. The result for the gas permeability and selectivity is presented in **Figure 4**(A).

First of all, it could be seen that the pristine PIM-1 has a gas permeability of around 4000 Barrer and the CO_2/N_2 ideal selectivity was found to be around 15. This result is comparable with previously published results with PIM-1 membrane.[39-40] Upon incorporation with the MOF at 5 wt% loading, the CO_2 permeability could be increased to around 6700 Barrer. This was also followed by improvement in CO_2/N_2 ideal selectivity to around 20. Upon increasing the MOF loading to be 10 wt%, the CO_2 permeability could be increased further slightly to be around 7500 Barrer while maintaining the selectivity around 19. For the PIM-1 MMM with the highest loading, namely 20 wt%, the CO_2 permeability could reach up to 10000 Barrer but with a slight compromise of decrease in CO_2/N_2 ideal selectivity to around 17. The slight reduction of the CO_2/N_2 ideal selectivity could be attributed to particle agglomeration resulting in the development of some micro-cracks formed at the MOF-polymer interface that was not obvious through SEM micrograph.[41] Despite this, all these results show the ability of the PIM-1 MMM to surpass the 2008 Robeson Upper Bound for CO_2/N_2 separation.[42] As in Matrimid-based MMMs, we also did a comparison study with the 10 wt% DMOF-1 – PIM-1. As also can be seen, the DMOF-1 – PIM-1 MMM showed an increase in CO_2 permeability to be around 7000 Barrer compared with the pristine PIM-1 which had 4500 Barrer. However, a difference regarding CO_2/N_2 separation factor could be observed. The CO_2/N_2 ideal selectivity of DMOF-1 – PIM-1 was found to barely increase to be around 13 as in pristine PIM-1. This improvement in ideal selectivity is then in agreement with the previous observation with DMOF-1 – Matrimid MMM.

To further investigate the promising result from PIM-1-based MMMs, equimolar mixed gas scenarios were also studied and the results are presented in **Figure 4**(A) (half-filled symbols). It could be seen that in the equimolar mixed gas condition, the CO_2 permeability decreased almost 20% for the pristine PIM-1 compared with the single gas condition. In addition, the CO_2/N_2

selectivity also decreased to around 10. This reduction in CO_2 permeability is more significant compared with some previous investigations[43-44] but is still consistent with some findings that observed reduction in CO_2 permeability and separation factor in a mixed gas scenario.[45-46] This could be attributed by different total pressure used during this study. It should be noted that the total pressure used in this study was around 1.5 bar (22 psia) during the single gas and mixed gas permeation study. As the gas permeation in PIM-1 membrane is highly dependent towards pressure, operation at lower pressure compared with the other studies might cause this phenomenon. In addition, there is also a possibility of competitive sorption between CO_2 and N_2 to be transported across the membrane during the mixed gas scenario resulting in lower membrane permeability and separation factor.[44]

A positive trend started to appear in the Azo-DMOF-1 – PIM-1 MMM. For an equimolar mixture of CO_2 and N_2, all of the MMM still exhibited similar behavior with the pristine PIM-1. About 25 % reduction in CO_2 permeability compared with the single gas measurement could still be observed. For the PIM-1 with the highest loading in particular, the CO_2 permeability could be maintained around at around 7600 Barrer, which is around 82% of the value obtained from the single gas permeation. However, a more positive impact could be observed for the CO_2/N_2 separation factor. The separation factor increased as more Azo-DMOF-1 was loaded in the PIM-1. For the equimolar feed of CO_2 and N_2, the separation factor increased by about 40% for the composite membrane with highest loading compared with the pristine PIM-1. This situation was barely observed when the PIM-1 was loaded with DMOF-1, in which case the separation factor was observed to be around 11. The 10 and 20 wt% Azo-DMOF-1 – PIM-1 MMMs were observed to have a separation factor around 13 and 14, respectively, showing that the performance started to plateau.

Compared with other relevant results in MOF- based mixed matrix membranes for CO_2/N_2 separation, the results obtained in this study are quite compelling. As can be seen in **Figure 4**(B), most studies in MMMs involving Matrimid, PIM-1 and other MOFs for CO_2/N_2 separation fall in the intersection of quadrant 1 and quadrant 4 regarding the permeability and selectivity improvement.[25, 45, 47-50] In this case, the MMMs are observed to have higher CO_2 permeability compared with the neat polymers but their selectivity barely change. Few MMMs could also be observed to fall between the intersection of quadrant 1 and quadrant 2. In this case, polymer chain rigidification and penetration into the MOFs could happen resulting in higher ideal selectivity but a slight compromise in CO_2 permeability. In an ideal situation, MOF-based MMMs are expected to show performance which is located at the upper right of quadrant 1. In this area, a beneficial interaction does exist between the MOF and the polymer resulting in both higher permeability and selectivity compared with the neat polymer. This condition could then be fulfilled as observed in this study by using Azo-DMOF-1 as the filler for the MMM. Both Matrimid and PIM-1-based MMMs show the similar trend, namely walking towards the upper right region of quadrant 1. This then shows the beneficial aspect of the azo-DMOF-1 compared with other MOFs including its parent structure, namely DMOF-1.

Although the difference between the Azo-DMOF-1 and DMOF-1 is only located on the presence of azobenzene group inside the MOF's pore, the performance behavior of the resulting MMMs were significantly different. A number of investigations have been attempted previously to predict and confirm the performance of DMOF-1 based membrane. For example, Erucar and Keskin have conducted a molecular study on DMOF-1 both in pure and composite membrane.[51] It is clear from their result that the MOF is only capable in enhancing the polymeric membrane CO_2 permeability without significant enhancement in selectivity. Although their study does not

include CO_2/N_2 separation performance, a similar trend (permeability improvement but stagnant selectivity) is confirmed by another study using the MOF in PDMS and polyimide matrix for CO_2/N_2 separation.[47] Despite the ability of the resulting composite membranes for getting close to the 2008 Robeson Upper Bound, the membranes only experienced improvement in CO_2 permeability and not selectivity. Furthermore, this phenomenon is not peculiar to the DMOF-1 MOF. A computational study has also been previously conducted to evaluate the performance of various MOFs for CO_2/N_2 separation in a composite membrane.[52] The result shows that only CO_2 permeability could be improved while selectivity remains unchanged which is also confirmed by other various studies which also confirms the location of the most of the MMMs performance that lies in the intersection of quadrant 1 and quadrant 4. Our study in DMOF-1 MMMs also confirmed this trend. As can be seen in **Figure 4**(C), the performance of DMOF-1 MMMs matched well with the predicted Maxwell model on permeability and selectivity with only a slight deviation observed. However, the Maxwell approach by using DMOF-1 system could not predict the performance of the Azo-DMOF-1 composites despite the only difference being the presence of azobenzene functionality where both permeability and selectivity of the MMMs are improved.

Since we observed different trends from most of the studies conducted on composite membranes, both diffusion and solubility coefficient values were calculated from the time-lag method[53] to obtain more insight on the effect of the azo MOF incorporation into the Matrimid and PIM-1 and the permeability and selectivity improvement. As can be seen in **Figure 4**(D), the diffusion coefficient of the resulting MMMs could be increased compared with the pristine membranes. The increase in diffusivity could be attributed to the increase of free volume from the incorporated MOFs that contributes in enhancing gas diffusion across the MMMs. However,

both CO_2 and N_2 experienced similar improvement in diffusion enhancement. This could be seen from the diffusion selectivity value that only increased slightly both in Matrimid and PIM-1 MMMs.

Meanwhile, a different situation could be observed for the solubility coefficient. Firstly, it could be seen that the solubility coefficient of the resulting MMMs decreased with higher particle loading. The gas diffusivity increase and solubility decrease were also previously observed in various mixed matrix membranes made from PEBAX,[54] Matrimid[55] and PIM.[45] This could be caused by lower gas solubility of the filler compared to the polymer resulting in an improvement of the solubility coefficient.[54] However, different from diffusivity selectivity, the decrease in solubility coefficient is accompanied by an increase in solubility selectivity for the MMMs used in this study. In membranes for gas separation, the solubility coefficient is related to the favorable thermodynamic interaction between the penetrant and the membrane. Therefore, the incorporation of the azo group in Azo-DMOF-1 framework might improve the affinity of the MMMs towards CO_2 rather than N_2 resulting in higher ideal selectivity. Previous investigations in the area of porous materials have also shown the beneficial aspect of having azobenzene functionality for CO_2/N_2 separation because of the ability of the azobenzene group with its nitrogen-rich environment to attract CO_2 through Lewis acid-base interaction and large quadrupolar moment.[26-27, 35] This study then further proves that the benefit of having azobenzene group in the MOF could be translated and useful in CO_2/N_2 membrane separation.

CONCLUSIONS.

In conclusion, we have successfully synthesized a new generation-2 light-responsive MOFs called Azo-DMOF-1. Compared to its parent, DMOF-1, the MOF has an azobenzene compound

protruding into the pore. Although a significant reduction of surface area was observed compared with the parent DMOF-1, the presence of azobenzene group was proven beneficial in improving the affinity between CO_2 and the framework as indicated by the enhancement of the CO_2 Q_{ads}. Interestingly, the presence of the azobenzene group in Azo-DMOF-1 is also beneficial in making the MOF to be photo-responsive towards CO_2 which is applicable for low-energy CO_2 capture. Further application was then explored by utilizing the MOF as a filler in a mixed matrix membrane. Both Matrimid and PIM-1 MMMs could be successfully fabricated using the Azo-DMOF-1 as the filler with various loadings. The performance test showed that both permeability and CO_2/N_2 selectivity could be significantly improved in the MMM incorporating the Azo-DMOF-1 which was not observed with the DMOF-1. For PIM-1 based MMMs in particular, the performance could surpass the 2008 Robeson Upper Bound indicating the promising performance of this particular MMMs for post combustion CO_2 capture application.

EXPERIMENTAL SECTION.

Synthesis of 2-phenyldiazenyl terephthalic acid (L1)

L1 was synthesized according to the published procedure with some modifications.[8] In a typical synthesis, 2.2 g of nitrosobenzene and 2.1 g of dimethylaminoterephthalate was dissolved in 85 mL glacial acetic acid in a round bottom flask. The solution turned to dark brown as reaction went on. The solution was then stirred for more than 3 days at 60°C under reflux. Afterwards, the solution was concentrated by evaporating the glacial acetic acid using a rotary evaporator. The concentrated solution was then neutralized using a saturated sodium hydrogen carbonate solution. The organic phase was then extracted using chloroform and concentrated under

vacuum. The crude product was purified using column chromatography (hexane : ethyl acetate : diethyl ether = 50:25:25) (1.33 g, yield 44%).

About 1.2 g of the resulting product was then dissolved in a mixture of 20% NaOH, THF and methanol (1:1:1). The reaction was stirred overnight at 50°C. The organic phase was removed and the aqueous part was acidified using 4M hydrochloric acid. The solid was then back extracted using diethyl ether which was then removed under vacuum to give an orange product (1 g, yield 92%). The purity of the ligand was confirmed by ^{1}H-NMR and mass spectrometer result as given in the Figure S1 and Figure S2, respectively, in the supporting information.

Synthesis of Azo-DMOF-1 and DMOF-1

Azo-DMOF-1 was synthesized by adapting the synthesis of its parent MOF $Zn_2(bdc)_2(dabco)$. In a typical synthesis, 0.11 g of $Zn(NO_3)_2.6H_2O$, 0.1 g of L1 and 0.022 g of DABCO were dissolved in 12 mL DMF through ultrasonication. The solution was then transferred into a glass vial and heated at 120°C for 2 days. The precipitate was then collected by filtration under vacuum and washed with DMF and DCM. The yield of the dried product was found to be around 39%. Azo-DMOF-1 was also then characterized using ^{1}H-NMR, TGA-MS and FTIR to confirm the successful synthesis of the new materials (see Supporting Information for the characterization details)

Meanwhile, DMOF-1 was synthesized according to the previously reported procedure.[12] In a typical synthesis, 0.11 g of $Zn(NO_3)_2.6H2O$, 0.061 g of terephthalic acid and 0.022 g of DABCO were dissolved in 12 mL DMF in a glass vial through ultrasonication. The vial was heated at 120^{o}C for two days. The products were collected by filtration and then washed with DMF and dichloromethane.

Fabrication of mixed matrix membranes

Matrimid and PIM-1 were used as the polymers for mixed matrix membrane fabrication. PIM-1 was synthesized according to the published procedure.[56] MMMs were fabricated with different particle loadings. In a typical fabrication, the required amount of particles and about 33% of the required amount of polymers were firstly dispersed in dichloromethane. After stirring for about 8 hours, the rest of the required polymer was added to the solution. The solution was then kept stirred overnight. Afterwards, the solution was poured into a petri dish and covered with perforated aluminum foil to evaporate the dichloromethane. For Matrimid-based MMM, this was followed by directly drying the membrane in the vacuum oven at 90°C for overnight. Meanwhile for PIM-1-based MMM, the membrane was soaked in methanol for 4 hours followed by overnight drying in vacuum oven at 85°C.

Nitrogen and CO_2 adsorption measurement

Both DMOF-1 and Azo-DMOF-1 was firstly activated under vacuum at 110°C before each measurement. Both nitrogen and CO_2 adsorption data were collected using Micromeritics 3Flex Instrument. The temperature for nitrogen sorption experiment was 77 K. The nitrogen sorption data was then used to calculate the pore width and pore volume according to the Horvath-Kawazoe model.[57] Meanwhile for the CO_2 adsorption, the two different temperatures were used: 273 and 298 K. Micromeritics ISO Controller filled with a 50:50 mixture of water and ethylene glycol was used to maintain the temperature during the measurement. The dynamic and static photoswitching of CO_2 adsorption were conducted using the previously published procedure.[6]

Mixed matrix membrane performance test

The membrane permeability was measured using a constant volume variable pressure approach. The complete description of the permeation has been previously published.[36]

For a mixed gas scenario, the gas rig was connected to the PerkinElmer Clarus 580 Gas Chromatograph (GC) to analyze the permeate composition. The columns installed in the GC are: (1) 7' HayeSep N 60/80, 1/8" Sf, (2) 9' Molecular Sieve 13x 45/60, 1/8" Sf, (3) 9' Molecular Sieve 5A 45/60 Sf and (4) 4' HayeSep T 60/80 Sf. The gas flow was controlled using mass flow controller purchased from Bronkhorst. For equimolar mixture, the CO_2 and N_2 flowrate were both maintained at 15 scm^3 min^{-1}. Meanwhile for the equimolar mixture scenario, the CO_2 and N_2 flowrate were both maintained at 15 scm^3 min^{-1}. The upstream pressure was maintained around 1.5 bar (22 psia) during the measurement and helium was used as the sweep gas at the permeate side flowing at 15 scm^3 min^{-1}. The schematic diagram of this test is given in Figure S6 in the supplementary information.

Other characterizations

Powder X-Ray Diffraction (PXRD) diffractograms were obtained using PAN-analytical instrument using Cu-Kα as the X-Ray source. The voltage and current was maintained at 40 kV and 20 mA, respectively, during the measurement. Measurement took place at ambient condition and the sample was spun. The diffractograms were collected between 5-40º in 2θ with 0.008º sample step.

Fourier Transformed Infrared Spectroscopy (FTIR) spectra were obtained using a Perkin-Elmer Spectrum 100 ATR-FTIR Spectrometer.

Thermal behavior of the samples were obtained using Netzsch STA 449 F5 Jupiter equipment. About 20 mg of sample was used both for MOF and the membranes. The heating rate was 5K min^{-1} under nitrogen atmosphere flowing at 20 ml min^{-1}.

SEM micrographs of the gold sputtered samples were acquired using a field emission gun scanning electron microscope (FEGSEM) Sigma 300 operated in secondary electron imaging mode at 5kV accelerating voltage. The working distance (WD) for the particles and membranes was 12 mm and 5-6 mm, respectively.

FIGURES.

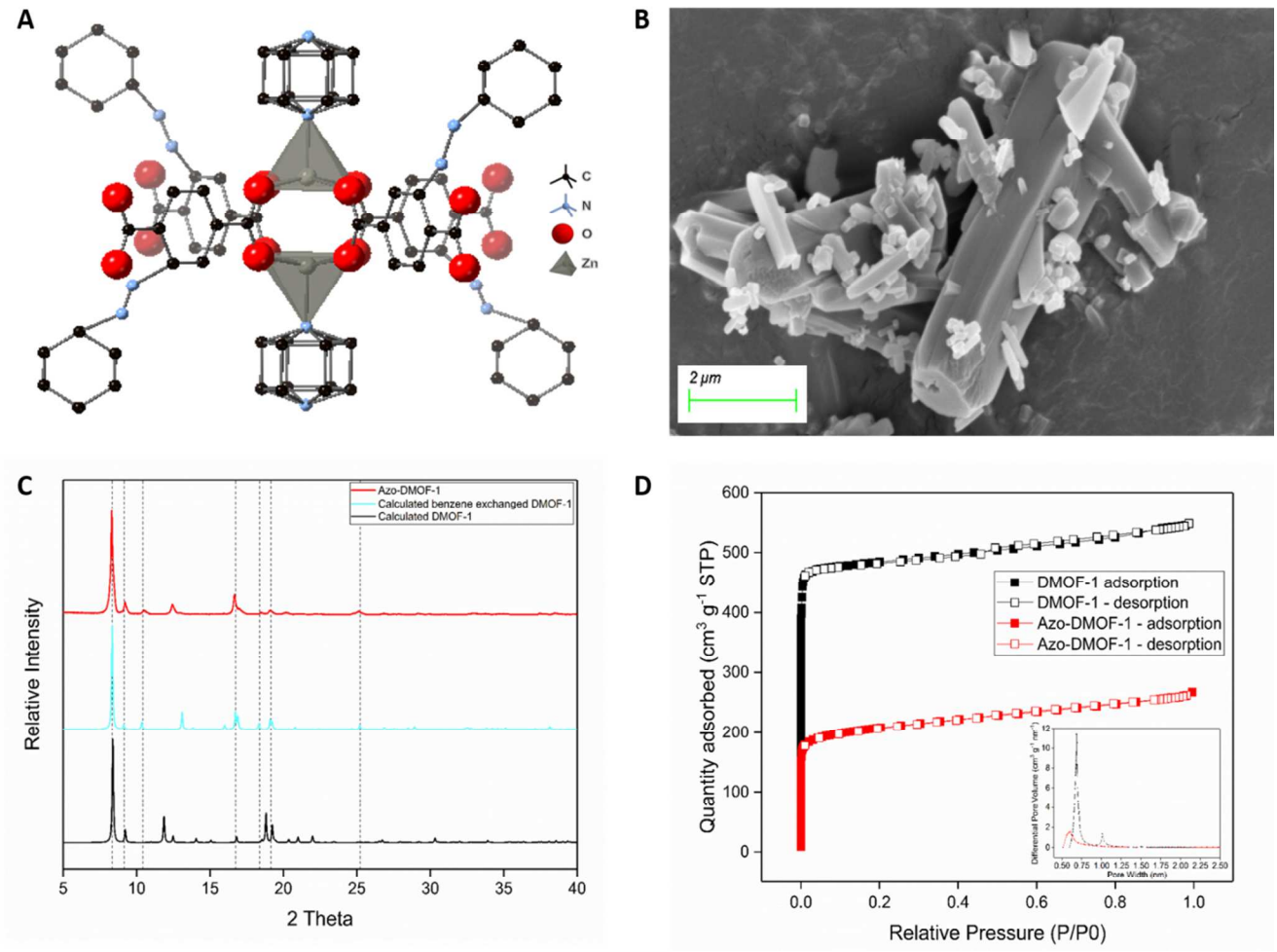

Figure 1. Hypothetical building unit (A), SEM micrographs (B), PXRD pattern (C) and N_2 sorption at 77K (D) of Azo-DMOF-1

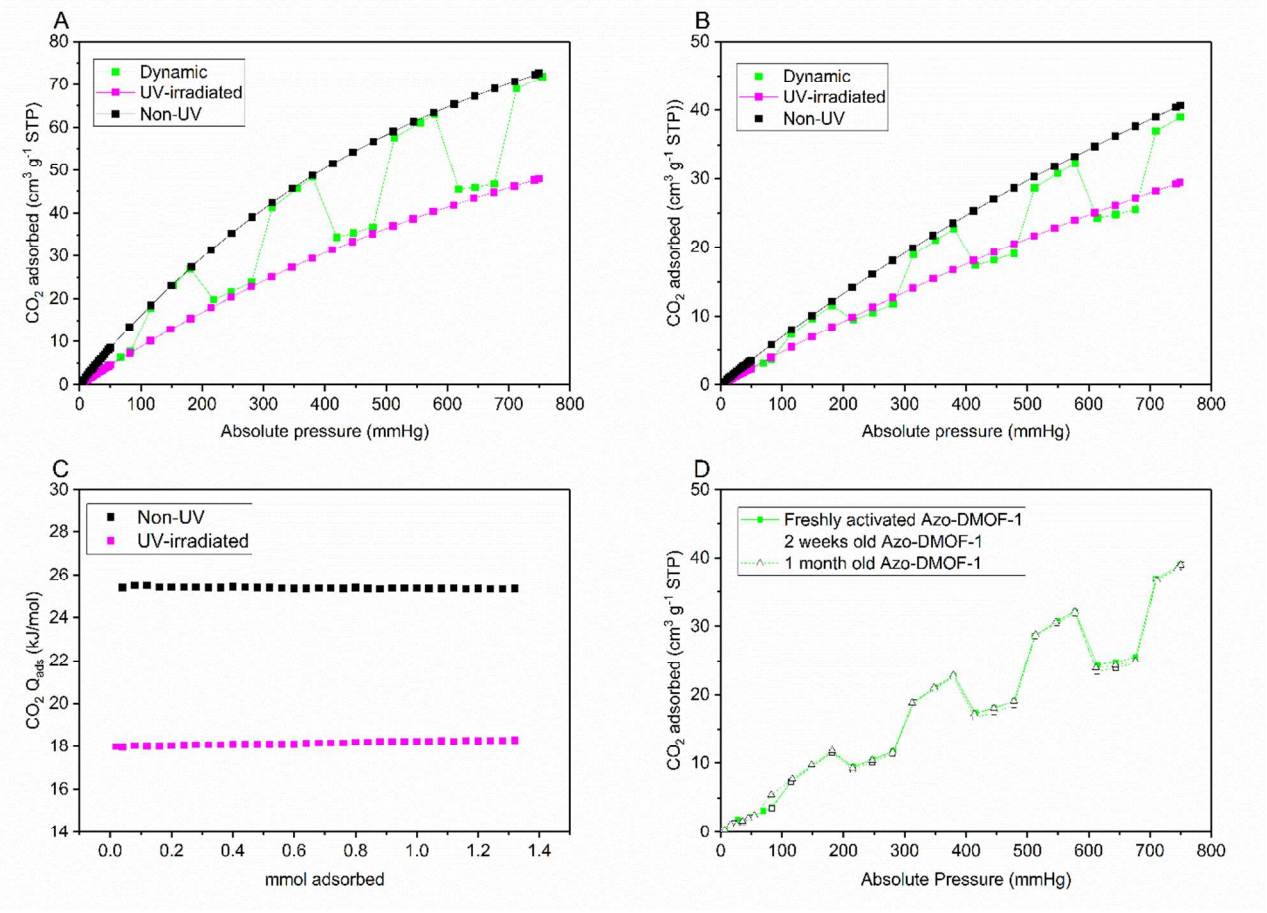

Figure 2. CO_2 adsorption of freshly-activated Azo-DMOF-1 and its dynamic photoswitching at 273 K (A) and 298 K (B), the isosteric heat of adsorption under normal and irradiated condition (C) and CO_2 adsorption stability test (D)

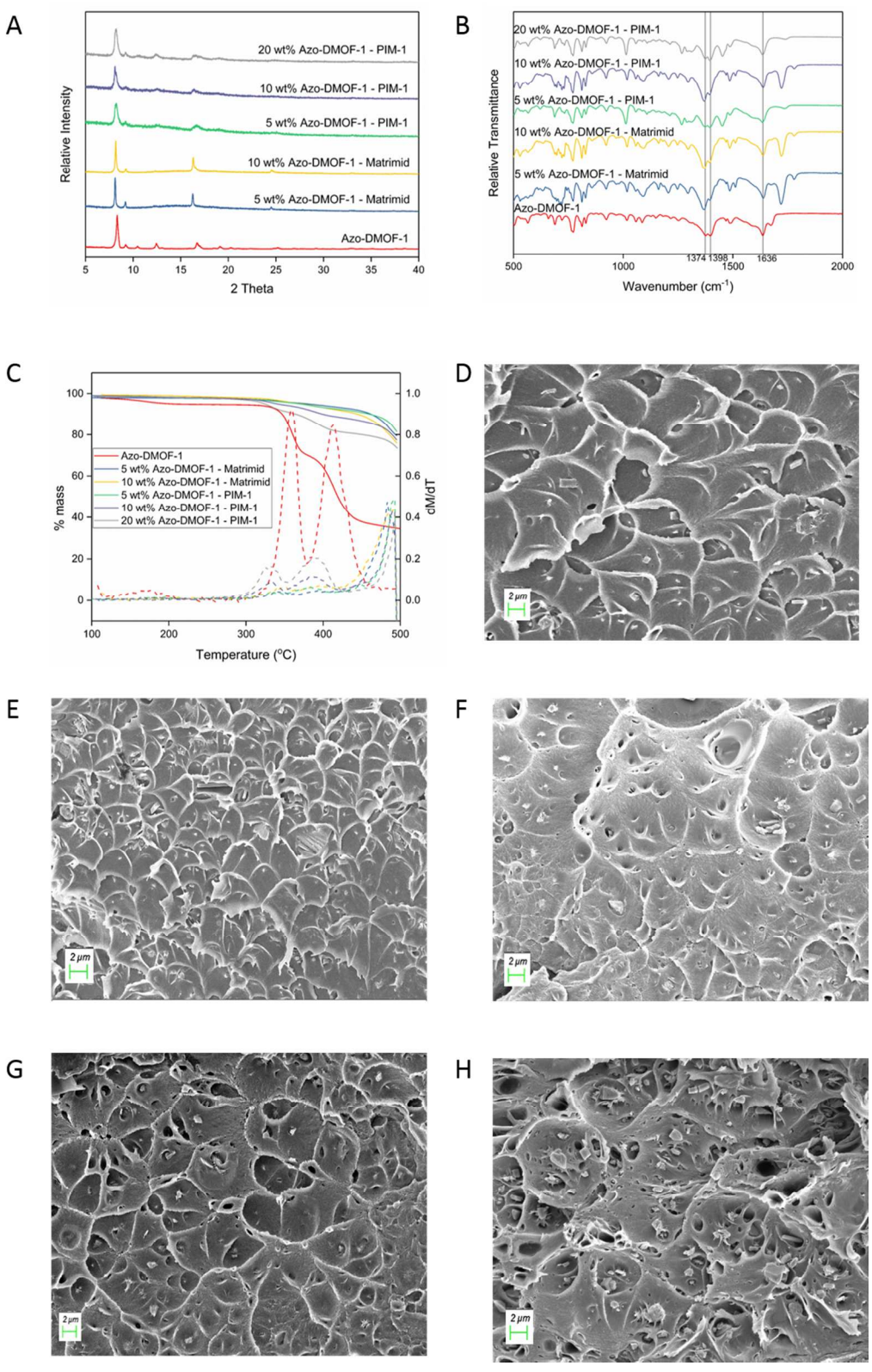

Figure 3. PXRD patterns (A), FTIR spectra (B) and thermal analysis (C) of the Azo-DMOF-1 MMMs and SEM micrograph pictures of: 5 wt% (D) and 10 wt% (E) Azo-DMOF-1 – Matrimid MMMs and 5 wt% (F), 10 wt% (G) and 20 wt% (H) Azo-DMOF-1 – PIM-1 MMMs.

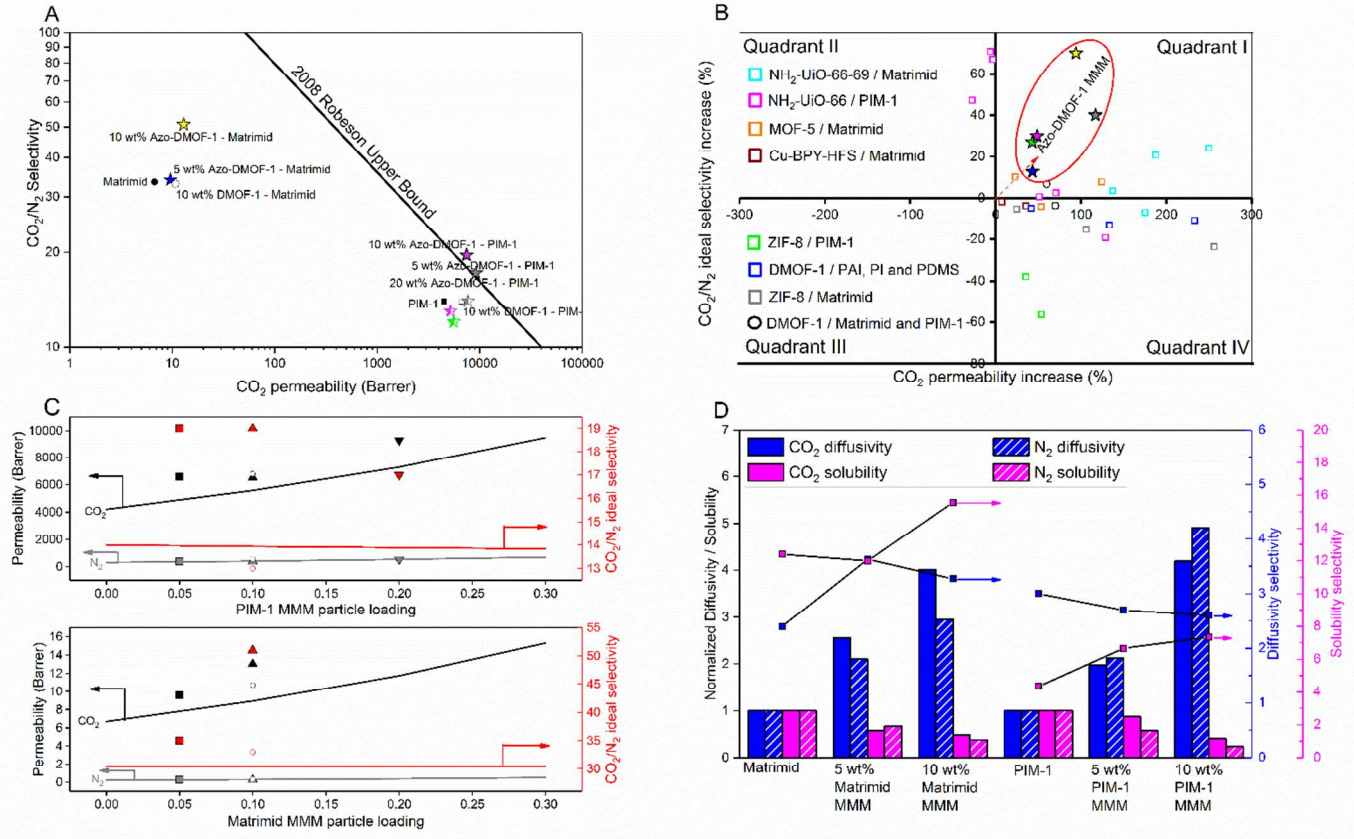

Figure 4. CO_2/N_2 separation performance of the Azo-DMOF-1 MMMs against 2008 Robeson Upper Bound (filled star: Azo-DMOF-1 MMMs pure gas performance, half-filled star: Azo-DMOF-1 mixed gas performance, empty symbol: DMOF-1 MMM performance) (A) and against other related MMMs [25, 45, 47-50] (B). Permeability and selectivity comparison against Maxwell equation using DMOF-1 MMMs (filled symbols: Azo-DMOF-1 MMMs, empty symbols: DMOF-1 MMMs) (C) and diffusivity and solubility coefficient analysis (D) of the Azo-DMOF-1 MMMs.

Displayed equations

Maxwell equation used in this study is described below

$$P_{mmm}=P_c\left[\frac{P_d+2P_c-2\emptyset(P_c-P_d)}{P_d+2P_c+\emptyset(P_c-P_d)}\right]$$

where P_{mmm}, P_c and P_d refer to gas permeability of the mixed matrix membrane, continuous phase (polymer matrix) and disperse phase (MOF) while Ø stands for the fraction of the filler in the continuous phase.

ASSOCIATED CONTENT

Supporting Information. Other characterizations for the DMOF-1 MOFs, control experiment for CO_2 photoswitching adsorption experiment and the value of diffusion and solubility coefficient of the mixed matrix membranes are available in the supporting information which can be accessed free of charge (file type: PDF).

Data Repository. The raw data used to produce all the graphs in this manuscript, the file used to produce Figure 1(A) in the CrystalMaker software, a high-resolution SEM image of Azo-DMOF-1 and a high-resolution version of Figure 1(A) are all freely available from the open repository: https://doi.org/10.5281/zenodo.1312360

AUTHOR INFORMATION

Corresponding Author

*Bradley P. Ladewig.

E-mail: b.ladewig@imperial.ac.uk

Author Contributions

NP and BPL planned the experiments. NP conducted all the experiments and data analysis. The manuscript was written through contributions of all authors. All authors have given approval to the final version of the manuscript.

ACKNOWLEDGMENT

NP acknowledges the PhD scholarship funding from the Department of Chemical Engineering, Imperial College London. NP gratefully acknowledges Dr. Piers Gaffney for his assistance during the ligand synthesis and Marcus Cook for preparing the PIM-1 which was used in this study. The assistance of Ms. Patricia Carry and Mr. Kaho Cheung for various analytical techniques is also acknowledged.

REFERENCES

(1) Moon, S.-Y.; Howarth, A. J.; Wang, T.; Vermeulen, N. A.; Hupp, J. T.; Farha, O. K. A Visually Detectable pH Responsive Zirconium Metal–Organic Framework. *Chem Commun* **2016,** *52*, 3438-3441.
(2) Ma, S.; Sun, D.; Wang, X. S.; Zhou, H. C. A Mesh□Adjustable Molecular Sieve for General Use in Gas Separation. *Angew Chem Int Ed* **2007,** *46*, 2458-2462.
(3) Li, H.; Sadiq, M. M.; Suzuki, K.; Doblin, C.; Lim, S.; Falcaro, P.; Hill, A. J.; Hill, M. R. MaLISA–a Cooperative Method to Release Adsorbed Gases from Metal–Organic Frameworks. *J Mater Chem A* **2016,** *4*, 18757-18762.
(4) Lyndon, R.; Konstas, K.; Ladewig, B. P.; Southon, P. D.; Kepert, P. C. J.; Hill, M. R. Dynamic Photo□Switching in Metal–Organic Frameworks as a Route to Low□Energy Carbon Dioxide Capture and Release. *Angew Chem Int Ed* **2013,** *52*, 3695-3698.
(5) Li, H.; Hill, M. R. Low-Energy CO2 Release from Metal–Organic Frameworks Triggered by External Stimuli. *Acc Chem Res* **2017,** *50*, 778-786.
(6) Prasetya, N.; Ladewig, B. P. Dynamic Photo-switching in Light-responsive JUC-62 for CO 2 Capture. *Sci Rep* **2017,** *7*, 13355.
(7) Ladewig, B.; Lyndon, R.; Hill, M., Gas separation processes. US Patent 9,533,282: 2017.
(8) Park, J.; Yuan, D.; Pham, K. T.; Li, J.-R.; Yakovenko, A.; Zhou, H.-C. Reversible Alteration of CO2 Adsorption upon Photochemical or Thermal Treatment in a Metal–Organic Framework. *J Am Chem Soc* **2011,** *134*, 99-102.
(9) Wang, Z.; Knebel, A.; Grosjean, S.; Wagner, D.; Bräse, S.; Wöll, C.; Caro, J.; Heinke, L. Tunable Molecular Separation by Nanoporous Membranes. *Nat commun* **2016,** *7*, 13872.
(10) Meng, X.; Gui, B.; Yuan, D.; Zeller, M.; Wang, C. Mechanized Azobenzene-functionalized Zirconium Metal-Organic Framework for On-command Cargo Release. *Sci Adv* **2016,** *2*, e1600480.
(11) Li, H.; Martinez, M. R.; Perry, Z.; Zhou, H. C.; Falcaro, P.; Doblin, C.; Lim, S.; Hill, A. J.; Halstead, B.; Hill, M. R. A Robust Metal–Organic Framework for Dynamic Light□Induced Swing Adsorption of Carbon Dioxide. *Chem Eur J* **2016,** *22*, 11176-11179.
(12) Dybtsev, D. N.; Chun, H.; Kim, K. Rigid and Flexible: A Highly Porous Metal–Organic Framework with Unusual Guest□Dependent Dynamic Behavior. *Angew Chem Int Ed* **2004,** *43*, 5033-5036.

(13) Liu, J.; Lee, J. Y.; Pan, L.; Obermyer, R. T.; Simizu, S.; Zande, B.; Li, J.; Sankar, S.; Johnson, J. K. Adsorption and Diffusion of Hydrogen in a New Metal− Organic Framework Material:[Zn (bdc)(ted) 0.5]. *J Phys Chem C* **2008,** *112*, 2911-2917.
(14) Xie, K.; He, Y.; Zhao, Q.; Shang, J.; Gu, Q.; Qiao, G. G.; Webley, P. A. Pd (0) Loaded Zn 2 (azoBDC) 2 (dabco) as a Heterogeneous Catalyst. *CrystEngComm* **2017,** *19*, 4182-4186.
(15) Savonnet, M.; Bazer-Bachi, D.; Bats, N.; Perez-Pellitero, J.; Jeanneau, E.; Lecocq, V.; Pinel, C.; Farrusseng, D. Generic Postfunctionalization Route from Amino-derived Metal− Organic Frameworks. *J Am Chem Soc* **2010,** *132*, 4518-4519.
(16) Wang, Z.; Cohen, S. M. Modulating Metal− Organic Frameworks to breathe: a Postsynthetic Covalent Modification Approach. *J Am Chem Soc* **2009,** *131*, 16675-16677.
(17) Wang, Z.; Tanabe, K. K.; Cohen, S. M. Accessing Postsynthetic Modification in a Series of Metal-Organic Frameworks and the Influence of Framework Topology on Reactivity. *Inorg Chem* **2008,** *48*, 296-306.
(18) Hahm, H.; Yoo, K.; Ha, H.; Kim, M. Aromatic Substituent Effects on the Flexibility of Metal–Organic Frameworks. *Inorg Chem* **2016,** *55*, 7576-7581.
(19) Henke, S.; Li, W.; Cheetham, A. K. Guest-dependent Mechanical Anisotropy in Pillared-layered Soft Porous Crystals–a Nanoindentation Study. *Chem Sci* **2014,** *5*, 2392-2397.
(20) Schneemann, A.; Takahashi, Y.; Rudolf, R.; Noro, S.-i.; Fischer, R. A. Influence of Co-Adsorbates on CO 2 Induced Phase Transition in Functionalized Pillared-layered Metal–Organic Frameworks. *J Mater Chem A* **2016,** *4*, 12963-12972.
(21) Yanai, N.; Uemura, T.; Inoue, M.; Matsuda, R.; Fukushima, T.; Tsujimoto, M.; Isoda, S.; Kitagawa, S. Guest-to-host Transmission of Structural Changes for Stimuli-responsive Adsorption Property. *J Am Chem Soc* **2012,** *134*, 4501-4504.
(22) Müller, K.; Knebel, A.; Zhao, F.; Bléger, D.; Caro, J.; Heinke, L. Switching Thin Films of Azobenzene□Containing Metal–Organic Frameworks with Visible Light. *Chem Eur J* **2017,** *23*, 5434-5438.
(23) Dong, G.; Li, H.; Chen, V. Challenges and Opportunities for Mixed-Matrix Membranes for Gas Separation. *J Mater Chem A* **2013,** *1*, 4610-4630.
(24) Erucar, I.; Yilmaz, G.; Keskin, S. Recent Advances in Metal–Organic Framework□Based Mixed Matrix Membranes. *Chem Asian J* **2013,** *8*, 1692-1704.
(25) Perez, E. V.; Balkus, K. J.; Ferraris, J. P.; Musselman, I. H. Mixed-Matrix Membranes Containing MOF-5 for Gas Separations. *J Memb Sci* **2009,** *328*, 165-173.
(26) Patel, H. A.; Je, S. H.; Park, J.; Jung, Y.; Coskun, A.; Yavuz, C. T. Directing the Structural Features of N2□Phobic Nanoporous Covalent Organic Polymers for CO2 Capture and Separation. *Chem Eur J* **2014,** *20*, 772-780.
(27) Patel, H. A.; Je, S. H.; Park, J.; Chen, D. P.; Jung, Y.; Yavuz, C. T.; Coskun, A. Unprecedented High-temperature CO2 Selectivity in N2-phobic Nanoporous Covalent Organic Polymers. *Nat commun* **2013,** *4*, 1357.
(28) Chen, Z.; Xiang, S.; Arman, H. D.; Li, P.; Zhao, D.; Chen, B. Significantly Enhanced CO2/CH4 Separation Selectivity within a 3D Prototype Metal–Organic Framework Functionalized with OH Groups on Pore Surfaces at Room Temperature. *Eur J Inorg Chem* **2011,** *2011*, 2227-2231.
(29) Burtch, N. C.; Jasuja, H.; Dubbeldam, D.; Walton, K. S. Molecular-level Insight into Unusual Low Pressure CO2 Affinity in Pillared Metal–Organic Frameworks. *J Am Chem Soc* **2013,** *135*, 7172-7180.

(30) Huang, R.; Hill, M. R.; Babarao, R.; Medhekar, N. V. CO2 Adsorption in Azobenzene Functionalized Stimuli Responsive Metal–Organic Frameworks. *J Phys Chem C* **2016,** *120*, 16658-16667.
(31) Castellanos, S.; Goulet□Hanssens, A.; Zhao, F.; Dikhtiarenko, A.; Pustovarenko, A.; Hecht, S.; Gascon, J.; Kapteijn, F.; Bléger, D. Structural Effects in Visible□Light□Responsive Metal–Organic Frameworks Incorporating ortho□Fluoroazobenzenes. *Chem Eur J* **2016,** *22*, 746-752.
(32) Xiang, S.; He, Y.; Zhang, Z.; Wu, H.; Zhou, W.; Krishna, R.; Chen, B. Microporous Metal-Organic Framework with Potential for Carbon Dioxide Capture at Ambient Conditions. *Nat Commun* **2012,** *3*, 954.
(33) Chaemchuen, S.; Zhou, K.; Kabir, N. A.; Chen, Y.; Ke, X.; Van Tendeloo, G.; Verpoort, F. Tuning Metal Sites of DABCO MOF for Gas Purification at Ambient Conditions. *Microporous Mesoporous Mater* **2015,** *201*, 277-285.
(34) Liang, Z.; Marshall, M.; Chaffee, A. L. CO2 Adsorption-based Separation by Metal Organic Framework (Cu-BTC) Versus Zeolite (13X). *Energy Fuels* **2009,** *23*, 2785-2789.
(35) Arab, P.; Parrish, E.; İslamoğlu, T.; El-Kaderi, H. M. Synthesis and Evaluation of Porous Azo-linked Polymers for Carbon Dioxide Capture and Separation. *J Mater Chem A* **2015,** *3*, 20586-20594.
(36) Prasetya, N.; Teck, A. A.; Ladewig, B. P. Matrimid-JUC-62 and Matrimid-PCN-250 Mixed Matrix Membranes Displaying Light-responsive Gas Separation and Beneficial Ageing Characteristics for CO 2/N 2 Separation. *Sci Rep* **2018,** *8*, 2944.
(37) Prasetya, N.; Donose, B. C.; Ladewig, B. P. A New and Highly Robust Light-responsive Azo-UiO-66 for Highly Selective and Low Energy Post-combustion CO 2 Capture and its Application in a Mixed Matrix Membrane for CO 2/N 2 Separation. *J Mater Chem A* **2018,** *6, 16390-16402*.
(38) Valero, M.; Zornoza, B.; Téllez, C.; Coronas, J. Mixed Matrix Membranes for Gas separation by Combination of Silica MCM-41 and MOF NH2-MIL-53 (Al) in Glassy Polymers. *Microporous Mesoporous Mater* **2014,** *192*, 23-28.
(39) Ahn, J.; Chung, W.-J.; Pinnau, I.; Song, J.; Du, N.; Robertson, G. P.; Guiver, M. D. Gas Transport Behavior of Mixed-Matrix Membranes Composed of Silica Nanoparticles in a Polymer of Intrinsic Microporosity (PIM-1). *J Memb Sci* **2010,** *346*, 280-287.
(40) Staiger, C. L.; Pas, S. J.; Hill, A. J.; Cornelius, C. J. Gas Separation, Free Volume Distribution, and Physical Aging of a Highly Microporous Spirobisindane Polymer. *Chem Mater* **2008,** *20*, 2606-2608.
(41) Dorosti, F.; Omidkhah, M.; Abedini, R. Fabrication and Characterization of Matrimid/MIL-53 Mixed Matrix Membrane for CO2/CH4 Separation. *Chem Eng Res Des* **2014,** *92*, 2439-2448.
(42) Robeson, L. M. The Upper Bound Revisited. *J Memb Sci* **2008,** *320*, 390-400.
(43) Lasseuguette, E.; Ferrari, M.-C.; Brandani, S. Humidity Impact on the Gas Permeability of PIM-1 Membrane for Post-combustion Application. *Energy Procedia* **2014,** *63*, 194-201.
(44) Kinoshita, Y.; Wakimoto, K.; Gibbons, A. H.; Isfahani, A. P.; Kusuda, H.; Sivaniah, E.; Ghalei, B. Enhanced PIM-1 Membrane Gas Separation Selectivity through Efficient Dispersion of Functionalized POSS Fillers. *J Memb Sci* **2017,** *539*, 178-186.
(45) Ghalei, B.; Sakurai, K.; Kinoshita, Y.; Wakimoto, K.; Isfahani, A. P.; Song, Q.; Doitomi, K.; Furukawa, S.; Hirao, H.; Kusuda, H. Enhanced Selectivity in Mixed Matrix Membranes for CO 2 Capture through Efficient Dispersion of Amine-functionalized MOF Nanoparticles. *Nat Energy* **2017,** *2*, 17086.

(46) Scholes, C. A.; Jin, J.; Stevens, G. W.; Kentish, S. E. Hydrocarbon Solubility, Permeability, and Competitive Sorption Effects in Polymer of Intrinsic Microporosity (PIM□1) Membranes. *J Polym Sci, Part B: Polym Phys* **2016,** *54*, 397-404.
(47) Fritsch, D.; Peinemann, K.-v.; Gomes, D. D. F., Composite Material, in particular Composite Membrane, and Process for the Production of the Same. US Patent 7,658,784: 2010.
(48) Dechnik, J.; Sumby, C. J.; Janiak, C. Enhancing Mixed-Matrix Membrane Performance with Metal-Organic Framework Additives. *Cryst Growth Des* **2017,** *17*, 4467-4488.
(49) Song, Q.; Nataraj, S.; Roussenova, M. V.; Tan, J. C.; Hughes, D. J.; Li, W.; Bourgoin, P.; Alam, M. A.; Cheetham, A. K.; Al-Muhtaseb, S. A. Zeolitic Imidazolate Framework (ZIF-8) Based Polymer Nanocomposite Membranes for Gas Separation. *Energy & Environmental Science* **2012,** *5*, 8359-8369.
(50) Zhang, Y.; Musselman, I. H.; Ferraris, J. P.; Balkus, K. J. Gas Permeability Properties of Matrimid® Membranes Containing the Metal-Organic Framework Cu–BPY–HFS. *J Memb Sci* **2008,** *313*, 170-181.
(51) Erucar, I.; Keskin, S. Separation of CO2 Mixtures Using Zn (BDC)(TED) 0.5 Membranes and Composites: A Molecular Simulation Study. *J Phys Chem C* **2011,** *115*, 13637-13644.
(52) Sumer, Z.; Keskin, S. Computational Screening of MOF-Based Mixed Matrix Membranes for CO2/N2 Separations. *JNanomater* **2016,** *2016*.
(53) Rutherford, S.; Do, D. Review of Time Lag Permeation Technique as a Method for Characterisation of Porous Media and Membranes. *Adsorption* **1997,** *3*, 283-312.
(54) Zhao, D.; Ren, J.; Wang, Y.; Qiu, Y.; Li, H.; Hua, K.; Li, X.; Ji, J.; Deng, M. High CO2 Separation Performance of Pebax®/CNTs/GTA Mixed Matrix Membranes. *J Memb Sci* **2017,** *521*, 104-113.
(55) Moghadam, F.; Omidkhah, M.; Vasheghani-Farahani, E.; Pedram, M.; Dorosti, F. The Effect of TiO2 Nanoparticles on Gas Transport Properties of Matrimid5218-based Mixed Matrix Membranes. *Sep Purif Technol* **2011,** *77*, 128-136.
(56) Cook, M.; Gaffney, P. R.; Peeva, L. G.; Livingston, A. G. Roll-to-roll Dip Coating of Three Different PIMs for Organic Solvent Nanofiltration. *J Memb Sci* **2018,** *558*, 52-63.
(57) Horváth, G.; Kawazoe, K. Method for the Calculation of Effective Pore Size Distribution in Molecular Sieve Carbon. *J Chem Eng Jpn* **1983,** *16*, 470-475.